2025 IEEE/SICE International Symposium on System Integration (SII)
January 21-24, 2025, Munich, Germany

Tight Clearance Peg-in-Hole Motion Planner Using Gripper with Flexible Joint and Differential Infinity Rotatable Function of Palm

Masanori Ueda[1], Tokuo Tsuji[2], Tatsuhiro Hiramitsu[2], Hiroaki Seki[2], Toshihiro Nishimura[2], Yosuke Suzuki[2] and Tetsuyou Watanabe[2]

***Abstract*— We propose a method for a peg-in-hole task with tight clearance using a gripper developed in this study. The compact gripper developed is equipped with a flexible joint and a differential mechanism that allows infinite palm rotation. The flexible joint allows fingertip movement in any direction and in precise assembly tasks, even under positional errors. The differential mechanism enables unlimited rotation of the gripper palm to accommodate various assembly tasks. The compact design of the gripper enables effective operation in narrow spaces. We successfully achieved a peg-in-hole configuration by aligning a peg with a hole by pressing and rotating it without complex control or hole searching. Subsequently, the alignment is corrected via state recognition using a force sensor. The effectiveness of the developed gripper and control method is confirmed experimentally.**

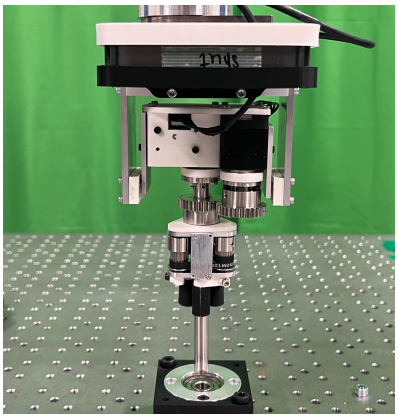

Fig. 1: Overview of our proposed gripper.

I. INTRODUCTION

Autonomous robotic assembly systems are crucial in various manufacturing fields, including the aviation [1] [2], automotive [3], and electronics industries [4], owing to the increasing demand for automation. Despite their prevalence, high-precision robotic manipulations cannot be achieved easily. Among the diverse assembly tasks, the peg-in-hole task has been widely researched because of its fundamental and versatile nature. Various methods haven been proposed, such as visual servo and force control.

The visual servo [5] uses camera feedback to guide the robot by detecting the positions of pegs and holes. However, this method is affected by variable lighting, camera calibration errors, and visibility issues as the peg approaches the hole, thus causing the hole to be obstructed. By contrast, the force-torque sensor allows one to determine the time at which the peg establishes contact with the edges of the hole, thereby providing essential feedback regarding the contact state and direction necessary for precise insertion. Methods for recognizing contact states include theoretical modeling, statistical analysis, and deep-learning applications [6].

Compliance control is essential for managing the uncertainty during peg-in-hole tasks. This control can be categorized into active and passive compliance, both of which adjust the robot's interactions to achieve successful insertion, even in tasks with uncertain errors. Active compliance control utilizes feedback from force-torque sensors to adjust servos, thus allowing robots to simulate the elasticity of springs to accomplish high-precision insertion tasks [7] [8]. However, this technique requires additional sensors, advanced servo systems, and complex algorithms and necessitating the processing of information from sensors, which inevitably introduces delays. By contrast, passive compliance control leverages the environment by incorporating a flexible joint into the robot, thus facilitating a simpler implementation while achieving comparable levels of softness [9] [10] [11] [12] [13]. Remote Center Compliance (RCC) [9] can align the tip of a peg with a hole using a compact mechanism, but it requires that the hole be chamfered. Additionally, a spiral search [14] [15] was proposed to search for holes using the robot's movement without a force-torque sensor. A spiral search with a flexible joint achieves high-precision insertions more efficiently [16]. However, this approach requires the movement of the robot body, thus potentially complicating control and limiting operation in narrow spaces. Besides these methods are not optimal for low-clearance peg-in-hole tasks and prolong the search time. Furthermore, Drigalski *et al.* [11] have reported cases of failure where the force signals were disrupted by noise in environments with uneven surfaces around the hole. Therefore, we developed the method that involves rotating a peg with a flexible joint to search for a hole [17]. This method enables fast circular peg-in-hole search without using sensors during hole searching. However, the developed method did not address a peg-in-hole task with tight clearance and the possible occurrence of jamming.

[1] M. Ueda is student of Graduate School of Natural Science and Technology, Kanazawa University, Kakuma-machi, Kanazawa-shi, Ishikawa 920-1192, Japan. masanoriueda0317@stu.kanazawa-u.ac.jp

[2] T. Tsuji, T. Hiramitsu, H. Seki, T. Nishimura, Y. Suzuki, and T. Watanabe are with Faculty of Frontier Engineering, Institute of Science and Engineering, Kanazawa University, Kakuma-machi, Kanazawa-shi, Ishikawa 920-1192, Japan. tokuo-tsuji, thiramitsu, hseki, tnishimura, suzuki, twata@se.kanazawa-u.ac.jp

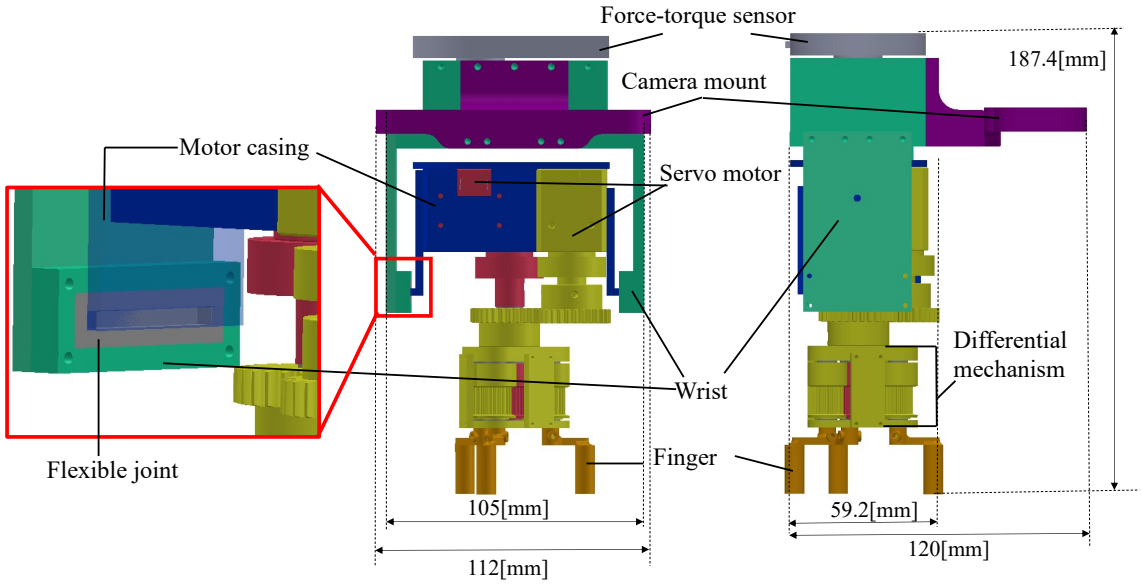

Fig. 2: 3D-CAD model of the gripper. The gripper consists of a main body, a wrist, a force-torque sensor, and three fingers. The main body houses two servo motors and a differential mechanism. The wrist is connected to the main body with flexible joints. The fingers utilize a rotary chuck mechanism.

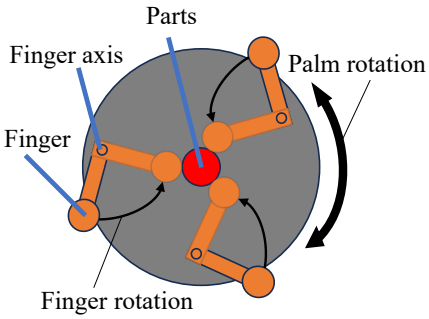

Fig. 3: Schematic of the finger movement. The opening and closing of the finger are achieved by rotating the axis located at the base of the finger.

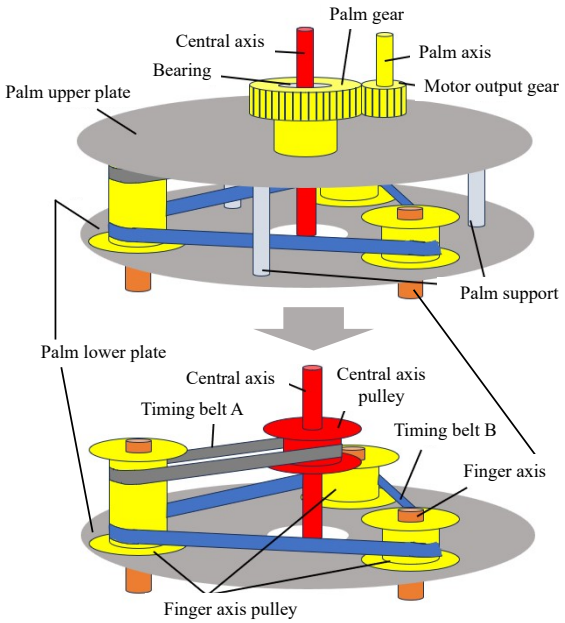

Fig. 4: Schematic of the differential mechanism that is composed of four pulleys and two timing belts. The diagram below depicts the palm plate removed from the upper diagram.

In this study, along with motion planning designed for peg-in-hole tasks with low tolerance and significant positional error, we introduce a new compact three-fingered gripper in Fig. 1. The planner integrates a force-torque sensor with rule-based control to adaptively manage the operations of the gripper. The planner comprises three phases: rapid and low-cost peg-and-hole mating, aligning the peg-and-hole orientation, and inserting the peg while rotating it. In the first phase, the peg is mated with the hole by merely rotating the peg without having to search for the hole position. In the second phase, the peg and hole are aligned using feedback from a force sensor and simple translational movement. In the third phase, peg insertion is facilitated with less force by pushing the peg while rotating it. The proposed gripper features a flexible joint and an infinitely rotatable palm. The flexible joint passively adjusts the alignment errors between the peg and hole. The infinite rotation mechanism enables the rotation of the peg itself which is facilitating alignment between the peg and hole. We assess the performance of our gripper and motion planner by inserting a shaft into a vertical bearing. The peg-in-hole setup used in our experiments indicates low tolerance; thus, it is susceptible to jamming owing to slight orientation errors.

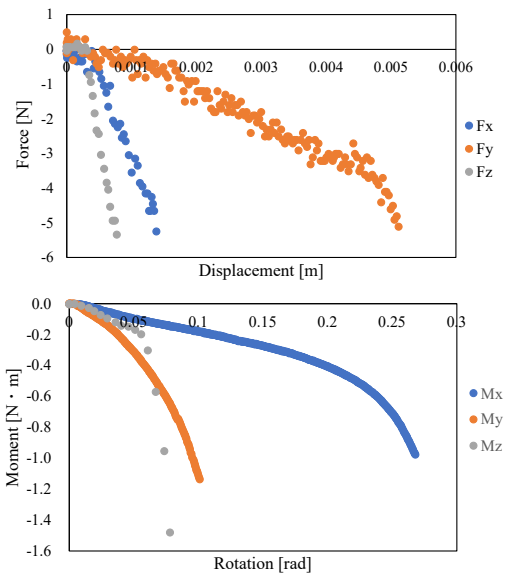

Fig. 5: Gripper's flexibility in response to force and moment. A gentler slope indicates greater flexibility in response to external forces. The upper section of the figure shows the graph of force versus displacement, while the lower section shows the graph of moment versus rotation.

II. Design of the Gripper

A. Overview

An overview of the three-dimensional computer-aided design (3D-CAD) model of the gripper is presented in Fig. 2. It integrates a force-torque sensor (FFS055YS102U6_S055F103, Leptrino) and a wrist directly mounted on the robot's main body, with flexible joints incorporated between the wrist and motor casing. The motor casing encloses two servomotors (XM430-W210-R, Dynamixel) and incorporates a differential mechanism that utilizes these motors. The grasping mechanism employs a rotary chuck, as described by Fukunishi *et al.* . [18], in which the rotation of the axis opens or closes the fingers, as shown in Fig. 3.

B. Differential Infinity Rotatable Function of Palm

Fig. 4 shows a schematic of the differential mechanism presented in Fig. 2. Infinite-rotation functionalities are typically implemented using slip rings, as reported by Tennomi *et al.* . [17]. However, slip rings are susceptible to degradation and contact failure owing to external forces. Hence, we mechanically implemented the infinite-rotation functionality using a differential mechanism.

In designing a rotary gripper [19], Hughes it et al. introduced an alternative method for achieving infinite rotation without using slip rings. The rotary gripper facilitates independent gripper opening and infinite rotation by employing a lead screw that tightens the constriction ring.

As shown in Fig. 2, the gripper features two servo motors: the red servo motor provides an output to the central axis,

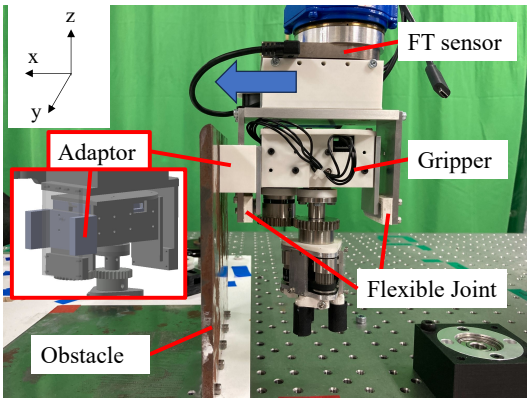

Fig. 6: A setup for Gripper's flexibility experiment. The robot continually collides the gripper with a fixed obstacle to obtain its position and force sensor readings.

whereas the yellow servo motor provides an output to the palm axis. At the end of the palm axis, the motor output gear is engaged with the palm gear affixed to the upper plate of the palm, thus enabling the yellow servo motor to rotate the palm. To prevent these rotational movements from interfering with one another, bearings were placed between the central axis and palm gear.

The lower section in Fig. 4 shows components concealed by the palm plate in the upper section of the same figure. A central axis pulley was fixed to the central axis, and each of the three finger axis pulleys was secured to their respective finger axes. Timing belt B was looped around all three finger axis pulleys, and timing belt A connected the central axis pulley to one of the finger axis pulleys.

When only the central axis was rotated, the relative speed of timing belt A with respect to the intermediate finger axis pulley matched the rotation speed of the central axis, thus causing all the finger axis pulleys to rotate. By contrast, when both the palm and central axes rotated at the same speed and in the same direction, the revolution and rotation speeds of the finger axis pulleys were the same. This resulted in a relative speed of zero for timing belt A with respect to the intermediate finger-axis pulley. Consequently, the fingers remained at their current spread while the palm performed infinite rotation.

C. Flexible Joint

Silicone rubber was used as the material for the flexible joints. As shown on the left side of Fig. 2, a component was introduced to envelop the protrusions on the left and right sides of the motor case. By incorporating this component as close as possible to the grippers center of gravity, position errors due to sagging during horizontal hand operations were minimized.

Fig. 5 shows the six degree-of-freedom flexibility of the flexible joint obtained experimentally. The experiment involved moving the robot until it collided with an obstacle to which the gripper was affixed as shown in Fig. 6; the force-torque sensor detected either 5.0 N or 1.0 N.m. The

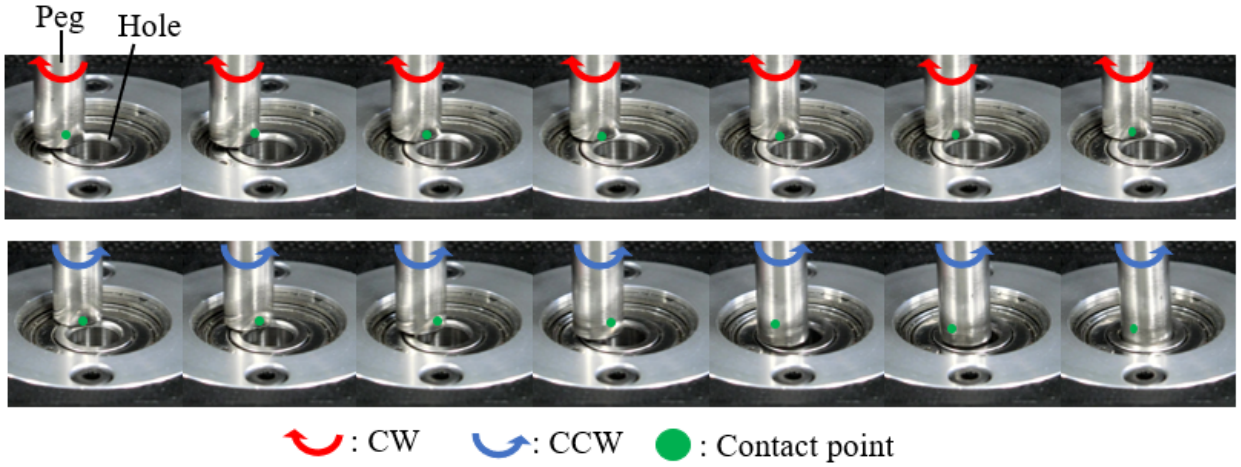

Fig. 7: An example where counterclockwise rotation leads to success.

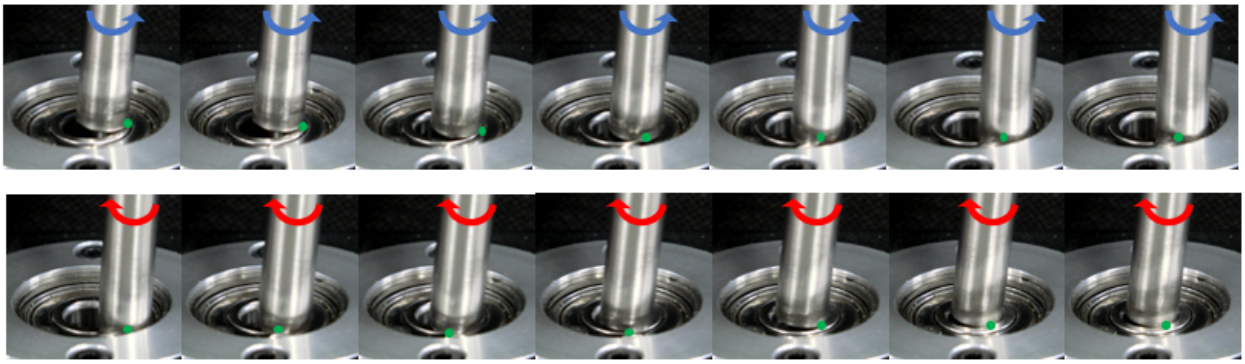

Fig. 8: An example where clockwise rotation leads to success.

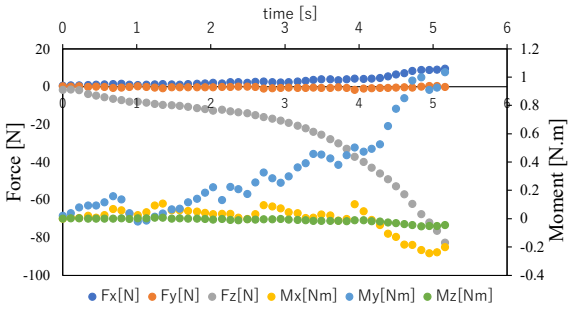

Fig. 9: Force and moment data obtained when jamming occurred.

force values, along with the position and orientation of the robot, were recorded every 0.1 s. To refer to the parameters of the most displaced parts in each graph, a displacement of 5mm is allowed for force, and a rotation angle of 0.25rad is allowed for moments.

III. Contact and Rotation

Tennomi *et al.* [17] proposed a strategy that involved using a flexible mechanism and rotating the peg itself to align it with the hole, demonstrating that merely rotating the peg enhanced the success rate. This approach eliminated the necessity for additional sensors and controls. However, they neither quantitatively assessed the effective range experimentally nor discussed solutions for addressing jammed pegs and holes.

The positional relationship between the hole and peg, as well as the tilt and rotation directions of the peg, influence its movement direction. As shown in Fig. 7, a peg that does not fit with clockwise rotation can be inserted by rotating it counterclockwise. Conversely, as the position of the peg changes, it may not fit with a counterclockwise rotation but can be inserted with a clockwise rotation, as shown in Fig. 8. Focusing on the contact points between the peg and the hole, which are plotted as green dots in Fig. 7, it can be observed that the peg moves around the contact point, and the contact point itself also shifts slightly. This phenomenon is referred to as contact and rotation (CaR) in the following discussion.

The flexible joint ensures the free movement of the peg within the motion range of the flexible joint, thus enabling CaR. When the peg was mated with the hole entrance, the initial pushing force caused the flexible joint to compress slightly, thus ensuring that the peg remained engaged and did not dislodge during subsequent rotations. The movement direction of the peg depends on its orientation and contact position with the hole. However, because the CaR duration is

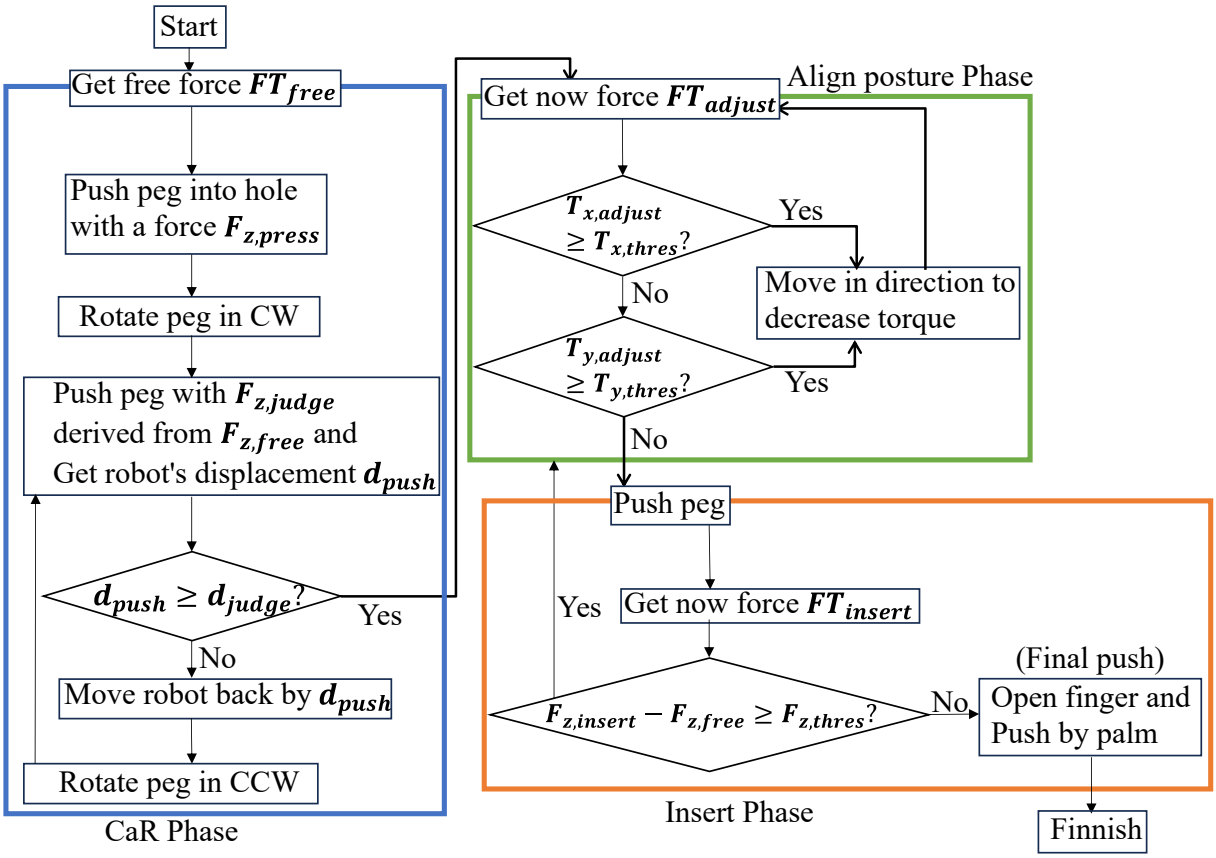

Fig. 10: Algorithm for peg-in-hole task.

extremely short, robust success can be achieved by rotating the peg clockwise and counterclockwise without having to measure the positional relationship.

IV. Peg-in-hole motion planner

In this study, we focused on peg-in-hole tasks with tight clearances. This scenario involved the insertion of a shaft into a bearing, which is similar to the operation during engine assembly. When the clearance is low, one must not only to align the positions of the peg and hole but also match their orientations. Proceeding with the insertion without aligning the orientation can lead to ”jamming, where the peg gets stuck partway through the hole. The tactile values presented in Fig. 9 were recorded when jamming occurred and the task could not be completed. Here, the hole is along the z-axis. Inserting a misaligned peg into the hole generated a moment from the forces at the contact points inside the peg and hole. Continued insertion under these conditions increases the resistance force owing to geometric constraints, thus rendering further insertion hazardous.

Hence, we implemented a rule-based motion planner that utilizes force feedback values to execute the task. The algorithms used in this planner are illustrated in Fig. 10. Here, we define the x- and y-axes as the two axes on the plane perpendicular to the hole, and the z-axis as the axis parallel to the hole. The planner comprises three phases: CaR, alignment, and insertion. The peg-in-hole process begins with the CaR phase, followed by the aligned-posture phase and then the insertion phase. If any adjustments are necessary, then the alignment-posture phase is repeated.

A. Phase 1: Contact and Rotation (CaR)

In the CaR phase, the peg and hole are mated and the success of the CaR is evaluated. In CaR, pegs and holes are aligned without the use of sensors, but the success is determined using force sensors. Initially, the force feedback value FT_{free} is obtained in the non-contact state. The peg is then brought into contact with the force $F_{z,\text{press}}$ and rotated clockwise. Next, the peg is pushed in the hole with a pressing-force feedback value $F_{z,\text{judge}}$ derived from $F_{z,\text{free}}$, and the displacement d_{push} in the z-direction is obtained. If d_{push} is less than the predetermined displacement d_{judge}, it is considered a failure. In this case, the d_{judge} was set to 2 mm, which is slightly smaller than the range of motion of the flexible joint. Conversely, if d_{push} is greater than d_{judge}, it is determined to be successful, and the process moves to the next phase. In the event of failure, the robot moves back according to the displacement made during the judgment and rotates counterclockwise before pushing again. If a successful judgment is obtained, the process advances to the next step; otherwise, it is terminated.

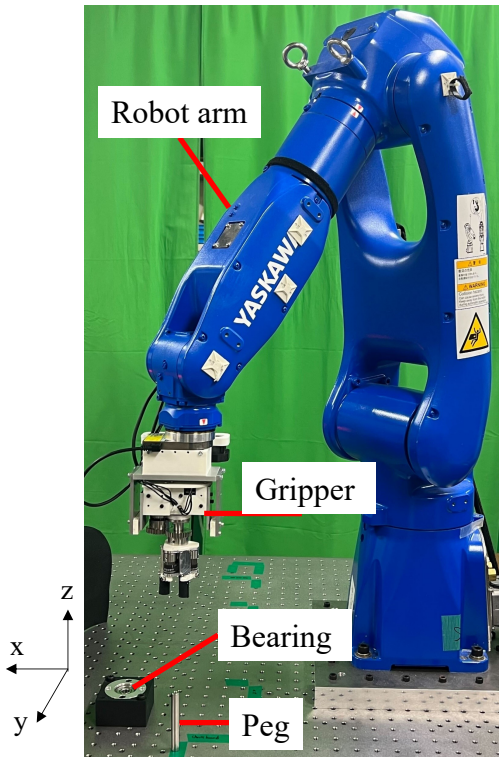

Fig. 11: Overall view of the experimental setup. The robot arm grips the peg and performs the peg-in-hole task with intentionally induced positional errors relative to the bearing hole.

B. Phase 2: Align posture

In the aligned posture phase, the peg and hole orientations are aligned along each axis. This alignment helps prevent jamming caused by the internal interaction between the peg and hole. First, the current force feedback value FT_{adjust} is obtained, and the moments around the x- and y-axes are extracted. If either of these moments exceeds the preset thresholds $T_{x,\text{thres}}$ and $T_{y,\text{thres}}$, the robot moves horizontally in a direction that reduces the exceeding moment, and the force feedback value FT_{adjust} is updated accordingly. If $T_{x,\text{thres}}$ is exceeded, move in the y-axis direction, and if $T_{y,\text{thres}}$ is exceeded, move in the x-axis direction. Once the moments around both axes are below their respective thresholds, the process proceeds to the next phase.

C. Phase 3: Insert

In the insertion phase, the peg is inserted and finally pushed into the hole. Periodically, the force feedback value in the z-direction, $F_{z,\text{insert}}$, is obtained and compared with the z-direction force component $F_{z,\text{free}}$ from FT_{free}. The difference is then checked against a predetermined threshold $F_{z,\text{thres}}$. If the difference does not exceed $F_{z,\text{thres}}$, this indicates that there is minimal force on the gripper, signifying that the orientations of the peg and hole are fully aligned. Conversely, if the difference exceeds $F_{z,\text{thres}}$, jamming occurs and the process returns to the aligned posture phase. When the difference no longer exceeds $F_{z,\text{thres}}$, the gripper fingers are opened, and a final push is performed with the palm to complete the peg-in-hole process.

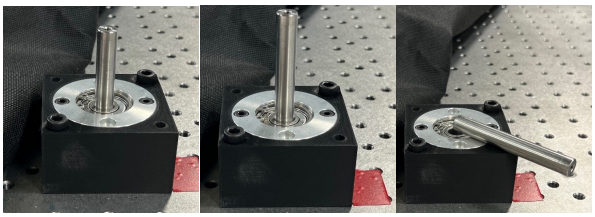

Fig. 12: Examples of success/failure determination in the experiment. (a) Success, (b) Jamming, and (c) Failure.

D. Pre-set parameters

The parameters were set as follows:

1. The pressing force during CaR $F_{z,\text{press}}$.
2. The pushing force for successful judgment during CaR $F_{z,\text{judge}}$.
3. The robot's displacement for CaR judgment is d_{judge}.
4. The threshold moment around the x-axis for the posture alignment is $T_{x,\text{thres}}$.
5. The threshold moment around the y-axis for the posture alignment is $T_{y,\text{thres}}$.
6. The force required for evaluating successful insertion is $F_{z,\text{thres}}$.

These six parameters must be appropriately configured for the system to function effectively.

V. TIGHT CLEARANCE PEG-IN-HOLE EXPERIMENT

A. Experimental Setup

We conducted experiments using a bearing holder with a diameter of 10 mm and an aluminum shaft with a diameter of 10 mm and a height of 75 mm. The tolerance of the hole is 10mm + 0.021mm, and the tolerance of the shaft is 10mm - 0.015mm, so the clearance between them was within 0.036mm.

In the experiment, as shown in Fig. 11, the bearing holder was fixed to a platform, and a robot arm (MOTOMAN-GP7, YASKAWA) grasping the peg was used for manipulation. The procedure is as follows: The robot was moved to a position above one of the grid points in a 7×7 grid with a spacing of 1 mm centered on the target hole. Subsequently, the robot traversed along the z-axis, which was aligned with the axis of the hole, thus enabling the peg to establish contact with the hole. Next, the robot performed the peg-in-hole task using the motion planner described in Section 4. The parameters introduced in Section 4D were statistically determined by repeatedly conducting experiments and acquiring data. For example, $F_{z,\text{press}}$ was determined to be 5N based on the force feedback values obtained during the CaR phase, and $T_{x,\text{thres}}$ and $T_{y,\text{thres}}$, which detect the misalignment between the shaft and hole, were set to 0.1Nm from Fig. 5. Additionally, to expedite the operation, the decision to perform the final push is made once $F_{z,\text{insert}}$ becomes almost equal to $F_{z,\text{free}}$. This

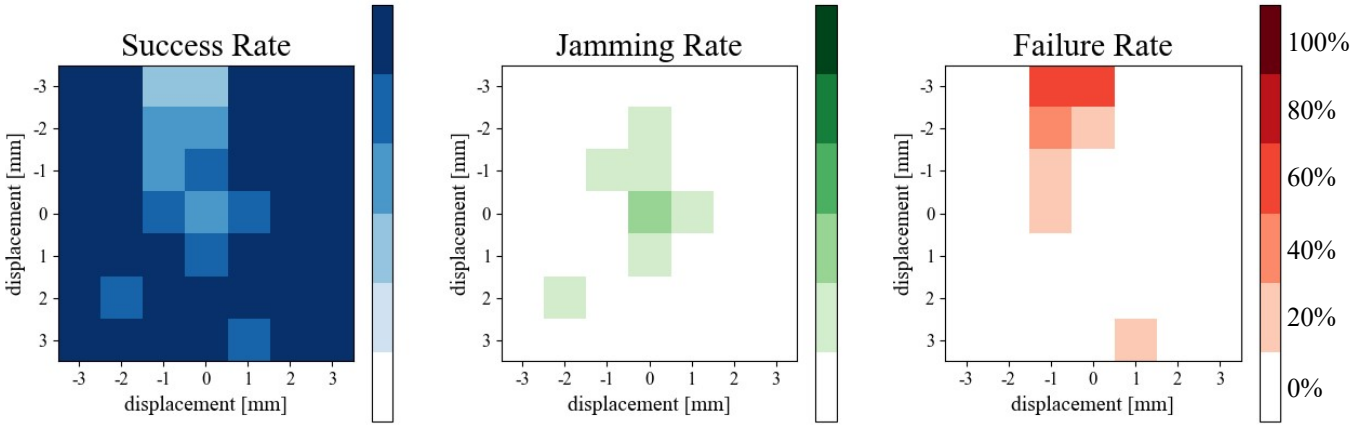

Fig. 13: Results of peg-in-hole experiment. For each grid, the rates of success, jamming, and failure are presented. Color shades indicate percentages, with darker colors corresponding to 100%, followed by 80%, 60%, 40%, 20%, and 0% respectively. Vertical and horizontal axes indicate positional errors relative to hole centers.

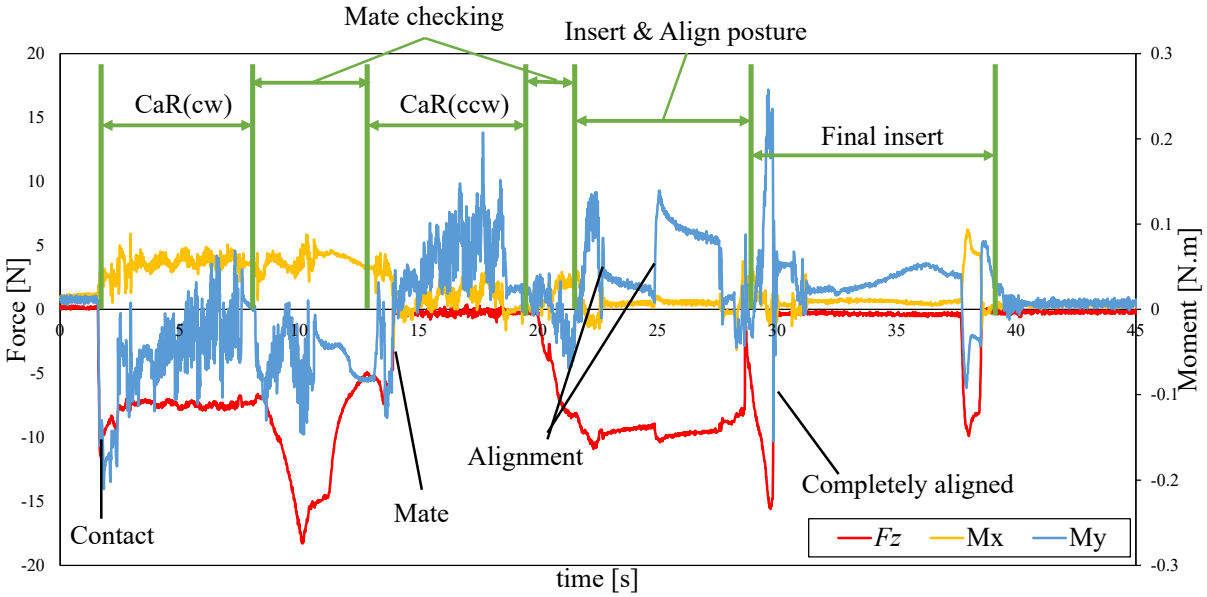

Fig. 14: Graph of data from the force sensor when successful peg-in-hole insertion was achieved via counterclockwise rotation. The parameters F_x, F_y, and M_z showed no significant changes and have been omitted.

assessment was conducted at various points after the peg established contact with the holes.

Finally, we conducted an evaluation using the assessment method shown in Fig. 12. A fully inserted peg is classified as a "Success", whereas a peg that becomes wedge halfway is termed as "Jamming." Meanwhile, a peg that fails CaR is labeled as a "Failure." The experiment was conducted in five sets, and the probabilities of success, jamming, and failure were calculated for each of the 7×7 tiles.

B. Results

The experimental results are shown in Fig. 13. Of the 245 trials conducted, we recorded 224 successes, 8 instances of jamming, and 12 failures. Among the jamming incidents, three were caused by failures in the successful CaR phase.

Jamming occurred more frequently near the center of the holes. This is attributable to the fact that the proximity of the peg to the hole center renders it difficult to detect jamming-induced moments at the onset of insertion. Additionally, the flexibility of the system may allow alignment with the hole without CaR, thus contributing to the phenomenon above. The bearings used have a passively moving inner ring, which resulted in longer exploration times by the CaR compared to cases where the area around the hole was fixed. The clustering of failures in specific areas is attributable to the characteristics of the gripper's flexible joints. This suggests that the mechanical properties of the joints may predispose certain regions to higher failure rates during insertion.

The graph shown in the Fig. 14 illustrates the data from the force sensor when peg-in-hole insertion was successful. Because there were no significant changes in F_x, F_y, and M_z, these parameters are not included in the description.

F_z is represented by a red line, M_x by a yellow line, and M_y by a blue line. During clockwise rotation with CaR, there was no engagement between the hole and the peg, thus F_z did not show significant variations, which indicates that the success detection was functioning appropriately. Subsequently, during counterclockwise rotation with CaR, the peg and hole mated, and F_z approached the force level observed in non-contact conditions, thus showing a change near zero. During the insertion phase, a rise in the moments indicated a transition to posture adjustment, followed by a decrease in moments.

VI. Conclusion

We proposed a rule-based motion planner that ensures successful peg-in-hole We proposed a rule-based motion planner that ensures successful peg-in-hole tasks, even with tight clearance and uncertain positional errors. This planner leveraged a low-cost, high-speed hole-searching method using CaR and simple posture alignment through force feedback. We developed a gripper equipped with a differential mechanism that enables the infinite rotation of the palm and flexible joints. The flexible joints allow the completion of challenging tasks with simple controls, demonstrating that the parameters set within the planner are independent of the task. Through experiments using grippers and planners, we quantitatively assessed the effective range of the CaR and confirmed that the pre-detection of jamming and alignment of the peg-in-hole successfully led to task completion.

In future work, to further enhance the robustness of the planner, we will conduct a theoretical model analysis of CaR, conduct a detailed examination of peg operations, and integrate the position correction mechanisms for failures encountered with CaR. Furthermore, regarding the success determination of the CaR, the current method based on the amount of insertion is prone to misjudgments near the center of the holes. Hence, plans are underway to develop a more accurate system that incorporates force sensing values alongside the current metrics. Additionally, by incorporating machine learning in the future, the success rate of tasks in various environments can be improved.

ACKNOWLEDGMENT

We would like to thank Editage (www.editage.jp) for English language editing.

References

[1] A. Wan, J. Xu, H. Chen, S. Zhang, and K. Chen, "Optimal path planning and control of assembly robots for hard-measuring easy-deformation assemblies," *IEEE/ASME Transactions on Mechatronics*, vol. 22, pp. 1600–1609, 2017.

[2] B. Mei and W. Zhu, "Accurate positioning of a drilling and riveting cell for aircraft assembly," *Robotics and Computer-Integrated Manufacturing*, vol. 69, p. 102112, 2021.

[3] M. Hebecker, J. Lambrecht, and M. Schmitz, "Towards real-world force-sensitive robotic assembly through deep reinforcement learning in simulations," *2021 IEEE/ASME International Conference on Advanced Intelligent Mechatronics (AIM)*, pp. 1045–1051, 2021.

[4] W.-C. Chang and C.-H. Wu, "Automated usb peg-in-hole assembly employing visual servoing," *2017 3rd International Conference on Control, Automation and Robotics (ICCAR)*, pp. 352–355, 2017.

[5] F. Chaumette and S. A. Hutchinson, "Visual servo control. i. basic approaches," *IEEE Robotics & Automation Magazine*, vol. 13, pp. 82–90, 2006.

[6] C. C. Beltran-Hernandez, D. Petit, I. G. Ramirez-Alpizar, and K. Harada, "Variable compliance control for robotic peg-in-hole assembly: A deep reinforcement learning approach," *ArXiv*, vol. abs/2008.10224, 2020.

[7] S. Kozlovsky, E. Newman, and M. Zacksenhouse, "Reinforcement learning of impedance policies for peg-in-hole tasks: Role of asymmetric matrices," *IEEE Robotics and Automation Letters*, vol. 7, pp. 10 898–10 905, 2022.

[8] Y. Gai, J. Guo, D. Wu, and K. Chen, "Feature-based compliance control for precise peg-in-hole assembly," *IEEE Transactions on Industrial Electronics*, vol. 69, pp. 9309–9319, 2022.

[9] D. E. Whitney, "Quasi-static assembly of compliantly supported rigid parts," *Journal of Dynamic Systems Measurement and Control-transactions of The Asme*, vol. 104, pp. 65–77, 1982.

[10] W. Haskiya, K. Maycock, and J. Knight, "A passive compliant wrist for chamferless peg-in-hole assembly operation from vertical and horizontal directions," *Proceedings of the Institution of Mechanical Engineers, Part B: Journal of Engineering Manufacture*, vol. 212, pp. 473 – 478, 1998.

[11] F. von Drigalski, K. Tanaka, M. Hamaya, R. Lee, C. Nakashima, Y. Shibata, and Y. Ijiri, "A compact, cable-driven, activatable soft wrist with six degrees of freedom for assembly tasks," *2020 IEEE/RSJ International Conference on Intelligent Robots and Systems (IROS)*, pp. 8752–8757, 2020.

[12] T. Nishimura, Y. Suzuki, T. Tsuji, and T. Watanabe, "Peg-in-hole under state uncertainties via a passive wrist joint with push-activate-rotation function," in *2017 IEEE-RAS 17th International Conference on Humanoid Robotics (Humanoids)*. IEEE, 2017, pp. 67–74.

[13] K. Tabata, T. Tsuji, A. Kawakubo, R. Kobayashi, T. Yamabe, Y. Suzuki, T. Nishimura, K. Yamazaki, T. Ishiti, and T. Watanabe, "Integrating force and vision feedback for flexible assembly system," in *Advanced Robotics*, vol. 37, no. 17, 2023, pp. 1100–1111.

[14] H. Park, J.-H. Park, D.-H. Lee, J.-H. Park, M. Baeg, and J.-H. Bae, "Compliance-based robotic peg-in-hole assembly strategy without force feedback," *IEEE Transactions on Industrial Electronics*, vol. 64, pp. 6299–6309, 2017.

[15] H. Park, J. Park, D.-H. Lee, J.-H. Park, and J.-H. Bae, "Compliant peg-in-hole assembly using partial spiral force trajectory with tilted peg posture," *IEEE Robotics and Automation Letters*, vol. 5, pp. 4447–4454, 2020.

[16] Q. Zhang, Z. Hu, W. Wan, and K. Harada, "Compliant peg-in-hole assembly using a very soft wrist," *IEEE Robotics and Automation Letters*, vol. 9, pp. 17–24, 2024.

[17] M. Tennomi, A. Okamura, Y. Nakamura, T. Abe, S. Wakamatsu, S. Tajima, T. Nishimura, Y. Hirai, T. Sawada, N. Ichikawa, T. Tsuji, K. Yamazaki, Y. Suzuki, and T. Watanabe, "Development of assembly system with quick and low-cost installation," *Advanced Robotics*, vol. 34, pp. 531 – 545, 2020.

[18] M. Fukunishi, H. Dobashi, and Y. Yokokohji, "Optimal design of rotational chuck-type hand with three parallel stick fingers for assembly tasks through grasp optimization," in *2021 IEEE/SICE International Symposium on System Integration (SII)*. IEEE, 2021, pp. 623–627.

[19] J. Hughes, K. Gilday, L. Scimeca, S. Garg, and F. Iida, "Flexible, adaptive industrial assembly: driving innovation through competition," *Intelligent Service Robotics*, vol. 13, pp. 169 – 178, 2019.